Cancer Imaging
the official publication of the International Cancer Imaging Society

MAKE YOUR *CANCER IMAGING* ARTICLE OPEN ACCESS

CANCER IMAGING publishes a mix of subscription-only articles (available only to paid subscribers) and OPEN ACCESS articles that are freely available to all.

By making your article open access, you will ensure that your article:

1. **Has a broader readership** – 13,000 readers per month, compared to 6000 non open access (figs from October 2008)
2. **Increased citation potential** as a result
3. **Complies with the requirements of grant-giving bodies**, who along with research institutions are now making funds available to cover open access

Open access articles are clearly flagged on the *Cancer Imaging* table of contents web page and are also immediately available on *PubMedCentral*.

Please **tick the box** if you wish to purchase open access for your article, and return with your proofs.

YES, I want to purchase open access for my *CANCER IMAGING* article

Title _____
Authors _____
Ref no _____

To make an article open access, authors are charged a per article fee of £350.

You may pay the open access fee online by going directly to our secure payment page at http://www.e-med.org.uk/securepayment.html and selecting the option 'Author purchase open access for individual article'.

Alternative methods of payment are available (e.g. by cheque); if you require a purchase order form or have any queries relating to payment, please email the publisher: marie.bardsley@e-med.org.uk

Cancer Imaging ◆ ISSN 1470-7330 (Online), 1740-5025 (Print) ◆
Published by e-MED Limited ◆ PO Box 61053, London SE16 7YZ, UK ◆ Tel: +44 (0) 20 7719 8989 ◆ Fax: +44 (0) 5601 264 446 ◆ E-mail: marie.bardsley@e-med.org.uk
www.cancerimaging.org

COPYRIGHT TRANSFER FORM

Each author is asked to transfer copyright to the **International Cancer Imaging Society**. This ensures international protection against unauthorised copying and reproduction in another electronic or print publication.

The publisher, e-MED, handles all requests from authors and third parties to reproduce all or part of any article published in *Cancer Imaging* (permissions@cancerimaging.org)

Title of article _____

_____

Author(s) _____

I/we hereby grant to the publisher for the full period of copyright, including any renewals or extensions throughout the World and in all languages, an exclusive licence to publish the above contribution or permit others to do so in print editions and in digital formats including online and network editions of the journal and in other derivative or collective works and to exploit subsidiary rights in the contributions including database rights.

By signing this form you certify that your contribution is your original work, has not been published before (in any language or medium) and is not being considered for publication elsewhere; that you have obtained permission for and acknowledged the source of any excerpts from other copyright works; that to the best of your knowledge your paper contains no statements which are libellous, unlawful or in any way actionable.

In return for the grant of exclusive licence, the contributor(s) (or, if copyright is vested in the contributor's employer, the contributor's employer) shall have the following rights:

> The right to reproduce a reasonable number of copies of the contribution, by downloading and photocopying for personal or professional (non-commercial) use. This use includes the contributor's own teaching purposes;
>
> The right to post, with the necessary acknowledgement and link to the *Cancer Imaging* web site, the contribution on the contributor's own, or contributor's institution's web site;
>
> The right to publish with the necessary acknowledgement all or part of the material from the published contribution in a book written or edited by the contributor(s). This does not apply to other articles in journals, for which permission must be sought.

The author signatory below represents that they sign this Agreement as authorised agents for and on behalf of all the authors.

Please return the completed form to production.manager@e-med.org.uk, or by fax to +353 61 280108, or by post to e-MED, Elva, Newquay, Burrin, Co Clare, Ireland.

Signed for and on behalf of all authors _____

Please print name _____

Date _____

Cancer Imaging (2011) **11,** S1–S17
DOI: 10.1102/1470-7330.2011.9034

CI

e-med
www.e-med.org.uk

Bony metastases: assessing response to therapy with whole-body diffusion MRI

A.R. Padhani and A. Gogbashian

Paul Strickland Scanner Centre, Mount Vernon Cancer Centre, Rickmansworth Road, Northwood, Middlesex, HA6 2RN, UK

Corresponding address: Dr Anwar Padhani, Paul Strickland Scanner Centre, Mount Vernon Cancer Centre, Rickmansworth Road, Northwood, Middlesex, HA6 2RN, UK.
Email: anwar.padhani@stricklandscanner.org.uk

Abstract

There are no universally accepted methods for assessing tumour response in skeletal sites with metastatic disease; response is assessed by a combination of imaging tests, serum and urine biochemical markers and symptoms assessments. Whole-body diffusion magnetic resonance imaging excels at bone marrow assessments at diagnosis and for therapy evaluations. It can potentially address unmet clinical and pharmaceutical needs for a reliable measure of tumour response. Signal intensity on high *b*-value images and apparent diffusion coefficient values can be related to underlying biophysical properties of skeletal metastases. Four patterns of change in response to therapy are described this review. Therapy response criteria need to be tested in prospective clinical studies that incorporate conventional measures of patient benefit.

Keywords: *Diffusion MRI; DW-MRI; WB-DWI; bone metastases; therapy response.*

Background

Metastatic bone disease is a common manifestation of advanced cancers with autopsy studies indicating a prevalence of 30–40% in thyroid, lung and renal cancers[1]. There is a greater prevalence of bony metastases in breast and prostate cancers (more than 70%)[1–3]. Bone metastases cause much of the morbidity and disability in patients suffering from tumours. Osteolytic disease in particular causes pain, impairs mobility, leads to hypercalcemia effects, results in pathological fractures and spinal cord compression. In patients with metastatic bony disease, survival rates vary by tumour type and can be months for lung cancer but can be years for hormone receptor positive disease in breast and prostate cancers[3].

Once bony metastases occur, cancer cure becomes impossible and therapy is instituted with palliative intent. Therapy goals are to delay progression, palliate symptoms, improve quality of life and achieve a modest survival benefit if possible. In general, systemic therapies (including chemotherapy, endocrine therapy and bisphosphonates) are given for disseminated disease and local treatments (e.g. radiotherapy, surgery and spine cement augmentation) to control pain and treat complications. Bisphosphonates reduce the frequency of skeletal-related events in breast cancer by 17–40%[4]. However, metastases do become refractory to bisphosphonate treatment and osteonecrosis and renal failure are recognized complications[5]. The recently introduced agent zoledronic acid, can reduce the incidence of skeletal-related events in both lytic and sclerotic disease[6]. The treatment of bony metastatic disease by targeting molecular mechanisms is an active research area[7]. Molecular targeted agents including HER2-neu inhibitors (trastuzumab) and RANK ligand inhibitors (denosumab) are helpful for the treatment of bony metastases[8].

Skeletal therapy assessment tools: comparison of methods

There are overwhelming clinical needs to develop and validate non-invasive response biomarkers for bone metastases[7–9]. There are, however, no universally accepted methods for assessing tumour response in skeletal sites with disease. Response is estimated by a combination of imaging tests, serum and urine biochemical

1470-7330/11/000001+017

markers, and clinical evaluations[10,11]. Symptom assessments (including analgesic requirements) and development of skeletal-related events are frequently used markers of therapeutic efficacy in clinical trials[10].

Serum markers of response are not available for the vast majority of tumours that metastasize to bone. Even serum prostate specific antigen (PSA) is not a completely reliable biomarker in late stage prostate cancer, especially in patients with hormone-refractory prostate disease[10]. A serum PSA flare phenomenon in responding patients has been noted[10]. Serum CA15-3 has moderate sensitivity for the detection of metastatic breast disease (60–65%)[12]. Similar to serum PSA, a CA15-3 flare reaction has been noted in responding breast cancer patients[13]. There are a number of serum and urinary markers of osteoblastic and osteoclastic activity that monitor bone response to the presence of metastatic disease[14], and thus only indirectly reflect disease activity of the metastatic bone marrow. Circulating tumour cells (CTCs) are emerging as powerful response biomarkers for breast, colorectal and prostate cancers[15]. Correlations of CTCs with tumour measurements on computed tomography (CT) and fluorodeoxyglucose (FDG)-positron emission tomography (PET) scans have been poor[16,17]. Correlations between CTCs and bony metastatic disease burden on FDG-PET have begun to emerge[18].

Bone scintigraphy ([^{99m}Tc]methylene diphosphonate (MDP) bone scans) with plain radiographs or cross-sectional imaging, such as CT or magnetic resonance imaging (MRI), remain the commonest imaging methods used to characterize and follow up bone marrow metastases. Unfortunately, bone scintigraphy reflects only on the osseous component of bone, and suffers from poor spatial resolution and limited diagnostic specificity, despite advances in single-photon emission computed tomography (SPECT). A positive bone scan occurs due to an osteoblastic response occurring secondary to an underlying bone abnormality and is thus an indirect indicator of metastatic bone marrow activity. Bone scintigraphy maybe unsuitable for the therapy assessment of predominantly lytic disease without an associated osteoblastic response such as typically seen in myeloma, renal or thyroid cancers (i.e. cold spots on bone scans cannot be followed for progression). Similarly patients with metastatic superscans on bone scans cannot be followed for progression. As a result, drug trials utilizing bone scans have criteria for progression (2 categories only: no new lesions/new lesions) but not for response; apparent progression need to be confirmed by follow-up bone scans after more than 6 weeks, when new focal hot spots have to be documented[10]. The latter observation raises the issue of timeliness of the bone scan readouts in patients who have to be continued on potentially ineffective therapies before progression can be documented. Scintigraphic/healing flare is also a well-recognized problem with bone scans occurring in 30% of patients usually within 3 months in patients responding to treatment[19,20].

CT scans are also limited in their ability to assess therapy response of bony disease. RECIST (v 1.1) criteria do allow individual osteolytic or mixed osteolytic/osteoblastic metastases to be measured but diffuse disease and osteoblastic bone metastases are considered as non-measurable[21,22]. The MD Anderson Cancer Center criteria (2004) introduced the concept of osteoblastic reaction as a response criterion when there are other signs of response and in the absence of progressive bony disease[11,21,23]. The appearance of new or worsening bone sclerosis on CT in patients with prostate cancer may therefore be erroneously classified as disease progression (CT flare response) and caution should be exercised in order to avoid over interpretation[24].

A number of PET tracers have been evaluated for their ability to monitor bony therapy response[25]. These include [^{18}F]sodium fluoride ([^{18}F]NaF), [^{18}F]fluorodeoxyglucose ([^{18}F]FDG), [^{11}C]/[^{18}F]choline (for prostate cancer), [^{18}F]fluoroestradiol ([^{18}F]FES); for hormone positive breast cancer), ^{68}Ga-labeled analogues of octreotide (e.g. [^{68}Ga] DOTATOC; for neuroendocrine tumours)[26,27]. A number of studies have shown that lytic bony disease is usually FDG avid and that many osteoblastic lesions are less FDG avid[28,29]. As a result FDG-PET scans may perform better in patients with breast cancer than in prostate cancer. FDG flare reactions occurring 7–10 days after tamoxifen therapy in estrogen receptor positive breast cancers can indicate eventual success[30]. An FDG flare reaction after growth colony stimulating factor (G-CSF therapy; given to prevent neutropenia-related complications) has been described and potentially may be difficult to distinguish from increasing bone marrow infiltration.

There are a number of MRI methods that can evaluate the bone for metastasis detection and response assessments[31,32]. Sequences relevant to the evaluation of bony metastases include T1-weighted (T1W) spin echo, T2-weighted (T2W, with fat suppression) and short tau inversion recovery (STIR) sequences, which are sensitive to the cellular, fat and water content of the bone marrow[33]. Gradient echo T1 sequences (in- and opposed phase imaging) can be used to evaluate the relative fat/water content of bone marrow. Susceptibility weighted (T2*) sequences can be made sensitive to susceptibility dephasing induced by trabecular bone[33]. Recently, ultrashort echo time sequences have been utilized to image trabecular bone structure in healthy and metastatic disease[34]. A number of studies have evaluated bone marrow vascularization using dynamic contrast-enhanced MRI techniques[35]. In the context of bone marrow assessment by metastatic disease, diffusion-weighted (DW) MRI is increasingly being used because it is sensitive to bone marrow cell density, the

relative proportions of fat and marrow cells, water content and bone marrow perfusion[35].

Whole-body DW imaging (WB-DWI) is emerging as an accurate bone marrow assessment tool for detection and therapy monitoring of bone metastases[32,36]. The major advantages of WB-DWI include the fact that no ionizing radiation is administered and no injection of isotopes or any contrast medium is necessary. Importantly, whole-body examinations are possible in reasonably short data acquisition times. The information obtained can be quantified and displayed as parametric maps, thus enabling spatial heterogeneity of tissues/tumours to be analyzed, before and in response to treatment. DW-MRI-derived parameters, such as the apparent diffusion coefficient (ADC), are theoretically independent of magnetic field strength and the relative simplicity of data acquisition facilitates multicenter and longitudinal studies[37]. In the rest of this article the imaging observations and mechanisms underlying the assessment of bony metastatic response to therapy with DW-MRI are discussed in depth[38].

DW-MRI correlations with bone marrow cellularity

Unlike the inverse correlations between ADC and cell density seen in many soft tissue tumours[39–49], ADC alterations in bone marrow as a consequence of metastatic disease are not inverse (Fig. 1) but the explanation for this observation is incompletely understood[50–53]. Yellow fatty marrow has lower cell density with an

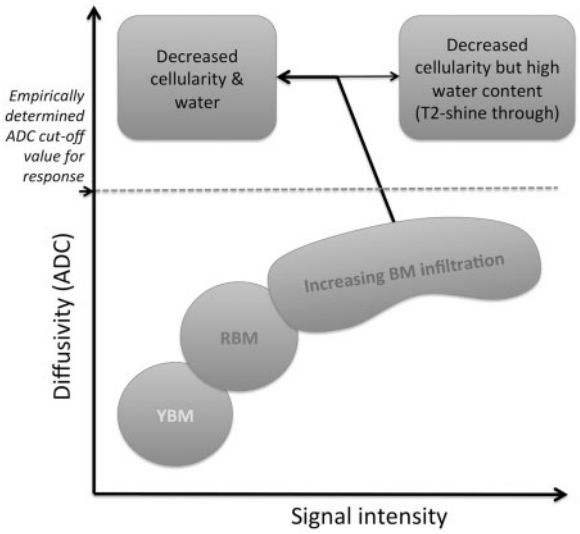

Figure 1 **Relationship between bone marrow diffusion signal intensity and ADC before and in response to successful therapy. An abundance of yellow bone marrow (YBM) fat causes low signal intensity on high *b*-value DW images. Increasing bone marrow cellularity of red bone marrow (RBM) and water content increases signal intensity and paradoxically increases ADC values also. Further increases in bone marrow cell density can cause lowering of ADC values although this is incompletely documented. Successful therapy results in increases in ADC values and decreases in signal intensity consistent with decreasing cellularity but T2-shine through effects following therapy would increase both signal intensity and ADC values.**

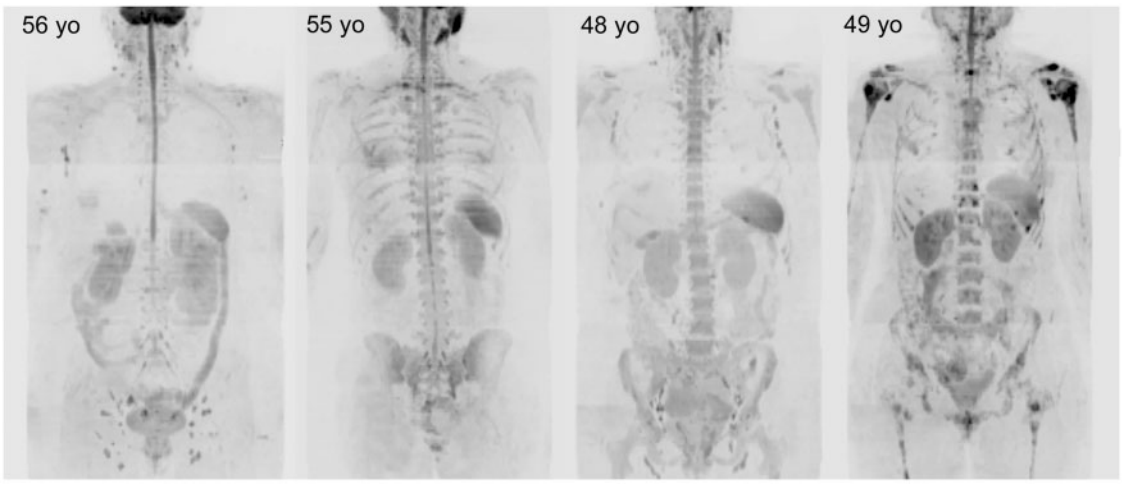

Figure 2 **Variable normal bone marrow signal intensity in women without and with metastatic disease. b900 3D-MIP (inverted scale) WB-DWI images of 4 middle-aged women with a history of breast cancer without metastatic bony disease (left 3 images) and with bony metastases (right side image). Ages are indicated (yo, years old). The first image shows a clearly outlined spinal cord with low signal intensity from the ribs and pelvic bone marrow indicating yellow bone marrow atrophy. The 4th right hand side image shows a woman with extensive bony metastases with multiple focal high signal intensity lesions in the axial skeleton. Asymmetry in the depiction of axillary nodes is due to nodal dissections. Other normal structures (kidneys, spleen, bowel, gall bladder) and soft tissue metastases (liver in the 1st image) are visible but not specifically annotated in these images.**

Table 1 Proposed DW-MRI response criteria for bone marrow lesions early after starting cytotoxic chemotherapy[a]

Signal intensity/ extent on high *b*-value images	ADC changes in relation to tumour-specific cut-off values[b]	Possible biological explanation and interpretation
↑	ADC values decrease, remain unchanged or increase but remain less than cut-off	Persistent hypercellularity → no evidence of response
↑	ADC values increase with most pixels greater than cut-off	Necrosis, hypocellularity, T2-shine through → evidence of response
↓	ADC values increase with most pixels greater than cut-off	Hypocellularity → evidence of response
↓	ADC values decrease or remain unchanged with most pixels less than cut-off	Possible sclerotic or fibrotic reaction → indeterminate for response

[a]Criteria may not apply to non-cytotoxic therapies. The timelines for the applicability of these criteria are undefined.
[b]ADC change needs to be judged in relation to cut-off values defined from untreated patients examined using the same imaging protocol. Cut-off values are likely to be dependent on tumour type.

abundance of fat cells compared with red bone marrow or metastatic disease. Yellow bone marrow has low signal intensity and low ADC values[50,54] probably because of the reduced proton density, the hydrophobic nature of fat and lower bone marrow perfusion (compared with red bone marrow)[55]. With increasing bone marrow cellularity (which displaces fat cells and increases the vascularity of the bone marrow), the signal intensity on high *b*-value images increases, and appears to paradoxically return higher ADC values compared with yellow bone marrow[52–54,56,57]. However, once all bone marrow fat cells are displaced, increasing bone marrow cell density within the confines of a fixed marrow space may cause ADC reductions (as in non-bone marrow tissues) but this latter effect has not been comprehensively documented.

WB-DWI: appearance of normal bone marrow

In order to use visual inspection of high *b*-value images for bone marrow metastasis detection, lesion characterization and for therapy assessments, it is necessary to be familiar with normal bone marrow distribution appearances on WB-DWI and to correlate findings with morphological sequences. Visual inspection of WB-DWI is excellent at demonstrating the variability of the normal bone marrow distribution. Variations in the cellularity of bone marrow are reflected in the signal intensity of the bones on high *b*-value images (Fig. 2). Because yellow bone marrow has low water content (10–20%)[58–60] its signal intensity on WB-DWI is reduced. On the other hand, red bone marrow has increased cellularity and water content (40–60%)[60,61], resulting in higher signal intensity on WB-DWI. The normal adult bone marrow distribution becomes established by 25 years of age with red bone marrow found predominantly in the axial skeleton and yellow bone marrow in the peripheral skeleton. There is variable red bone marrow atrophy and trabecular bone loss after 40 years of age[62] particularly in women (possibly related to estrogen deficiency and osteoporosis[63]), resulting in increased adiposity and thus lowering signal intensity of bone marrow on WB-DWI with increasing age.

There are many causes of bone marrow hypercellularity and hypocellularity observed in cancer patients too numerous to be elucidated in this article[36]. Common causes of bone marrow atrophy include chemotherapy and radiation treatment. A potential area of difficulty in assessing the bone marrow is the effect of haemopoetic growth factors such as granulocyte colony stimulating factor (G-CSF). G-CSF administration during chemotherapy results in increased signal intensity on WB-DWI that can mimic disease progression[64]. This is due to increases in bone marrow cellularity and water. The effects on bone marrow signal can occur within 2 weeks of the first G-CSF dose[65] but it is unclear whether additional doses further alter bone marrow signal intensity or whether there is resolution of changes on cessation of therapy. It is therefore potentially challenging to differentiate between new pathological bone marrow infiltrations and the benign red marrow reconversion changes related to G-CSF. Furthermore, bony metastases can become less conspicuous with increasing background bone marrow signal intensity due to G-CSF, making therapy assessments more difficult.

WB-DWI for skeletal metastasis detection

WB-DWI is an attractive lesion detection technique because it enables at a glance assessments, immediately drawing attention to potential abnormal skeletal regions (Fig. 2) and thus helping to reduce image interpretation times of anatomic WB-MRI[66]. WB-DWI can be considered to be a supplement for anatomic WB-MRI for improving skeletal lesion detection[67]. WB-DWI excels at lesion detection in the bone marrow, being better than CT scans and bone scans for detecting bony disease[54,68–70]. Skeletal metastases are

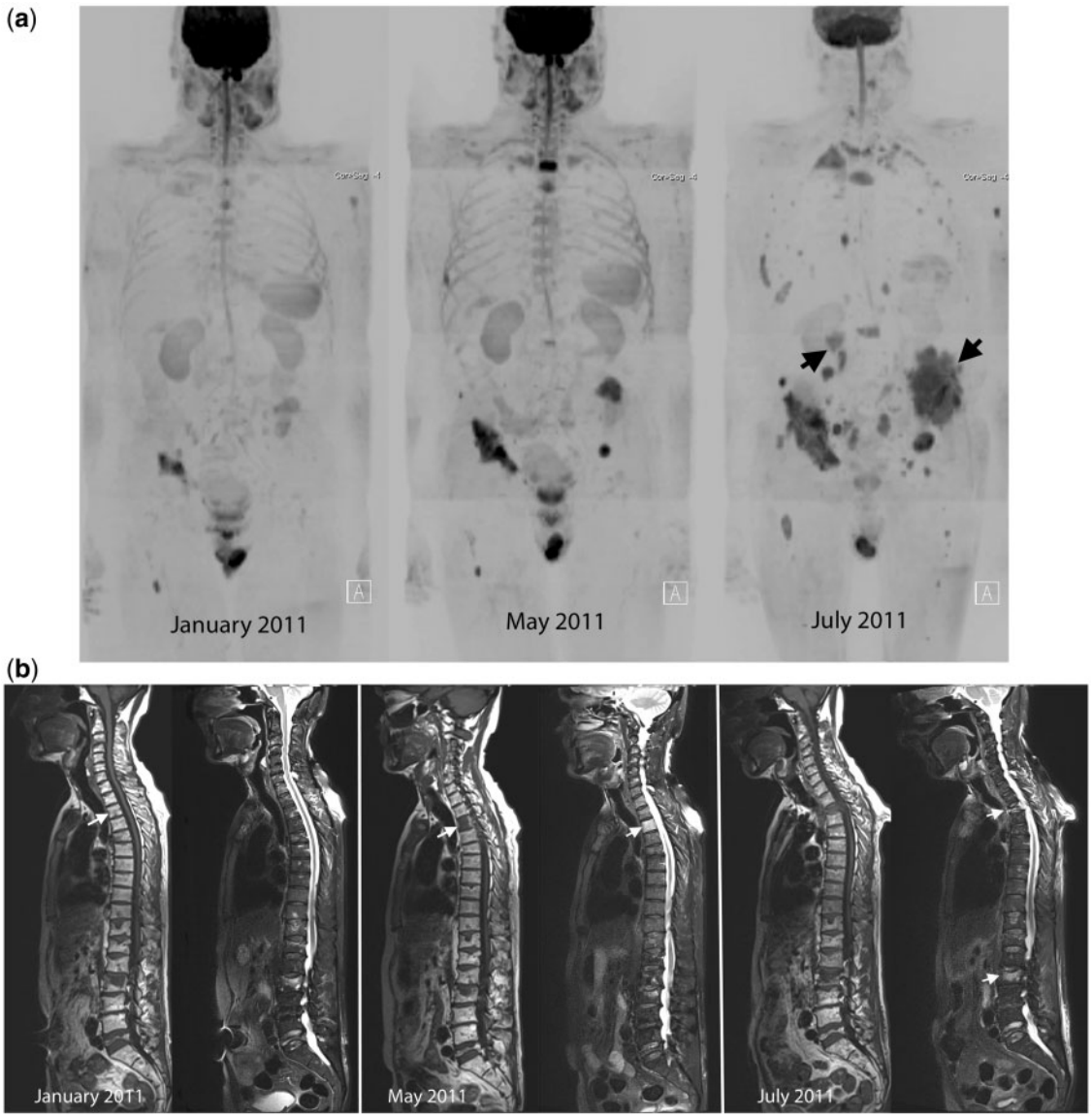

Figure 3 **Disease progression in multiple myeloma. A 69-year-old man with multiple myeloma. Disease progression despite treatment with lenalidomide and dexamethasone. (a) Serial b900 3-MIP (inverted scale) images. There are progressive increases in signal intensity over time despite therapy, particularly noticeable in the bony pelvis. New areas of bony disease involvement are also seen (ribs, left femur, pelvis). There is extra-osseous soft tissue disease at the right renal hilum and around the expanding left iliac bony lesion (arrows). General signal intensity reductions of the background bone marrow suggesting atrophy are also noted. (b) Serial whole spine sagittal T1W and T2W images. The subtle textural change of the D3 vertebral body seen on the January 2011 (arrow) study enlarges considerably in May 2011, signifying progression of disease (middle panel arrow). Other lesions remain relatively stable in appearance apart from some loss in height of D5. By July 2011, there is marked loss in height of D3 (last panel, top arrow) and increasing myelomatous infiltration at L2 (last panel, lower arrow). There is a collapse of the L5 vertebral body. (c) Axial b900 (left column) and ADC maps (right column) through the pelvis showing disease progression of the left iliac bone lesion. In January the lesion shows high signal intensity on the high *b*-value image and on the ADC maps (mean ADC 1915 $\mu m^2/s$; SD 252) consistent with T2-shine through (arrows). Progressive increase in tumour signal intensity extent can be seen with extra-osseous soft tissue tumour associated with decreases in ADC values (middle and lower rows; May: mean ADC 1133 $\mu m^2/s$ (SD 420) and July 1040 $\mu m^2/s$ (SD 285)).**

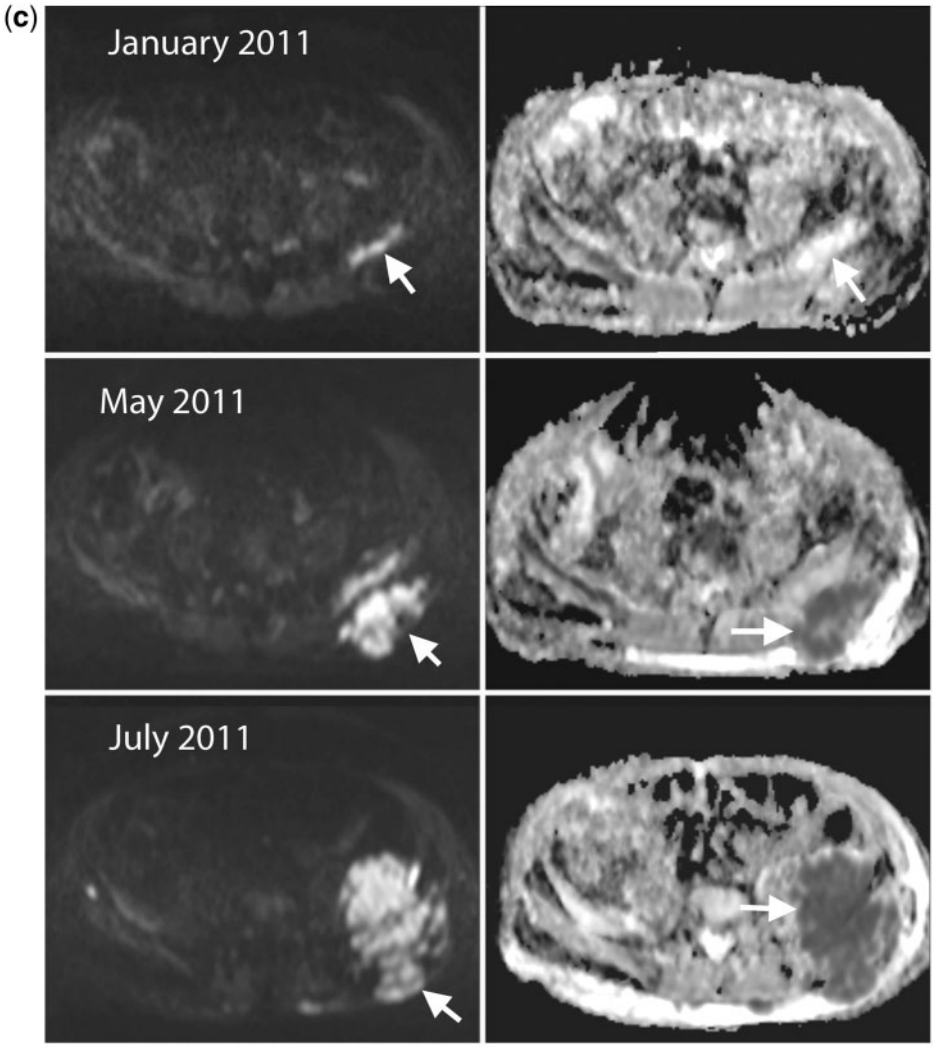

Figure 3 **Continued.**

recognized by focal/multifocal or diffuse, irregular-shaped high signal intensity regions within the bone marrow.

In a recently published meta-analysis, the ability of WB-DWI to improve sensitivity for bony metastasis detection was shown to be at the expense of a slight reduction in specificity[71]. Causes of false-positive increases in skeletal signal intensity on DWI images include bone marrow oedema caused by trauma[72], degenerative joint disease, bone infarction, infection and hemangiomas. Other causes of false-positive focal increases in signal intensity on DWI include isolated red bone marrow islands within yellow marrow and treated, but inactive metastatic lesions (T2-shine through). In order to avoid misinterpretations arising from signal intensity assessments alone, it is necessary to correlate high *b*-value images with corresponding ADC values taking into account morphologic features on other MRI sequences. T2-shine though effects can be reduced by increasing the strength of *b*-value gradients but this is at the expense of increasing image noise.

There are skeletal blind spots where lesion detection is impaired (potentially leading to false-negative results). These include metastatic lesions in the bone marrow of the anterior ribs and within the sternum which are sometimes relatively less conspicuous than lesions found in the spine and paraspinal regions. At these sites, complex incoherent motion contributes to signal losses on high *b*-value images. Other causes for false-negative results in bone marrow tumour detection include low levels of tumour infiltration, skull vault and skull base metastases (due to the adjacent high signal intensity of the brain) and when metastases develop within hypercellular bone marrow. As a general rule, lytic bony metastases are better seen than pure sclerotic metastases because of lower water and cellular content of sclerotic and treated lesions[54,73]. As a result, purely sclerotic bone metastases that are not visible on WB-DWI are not assessable for

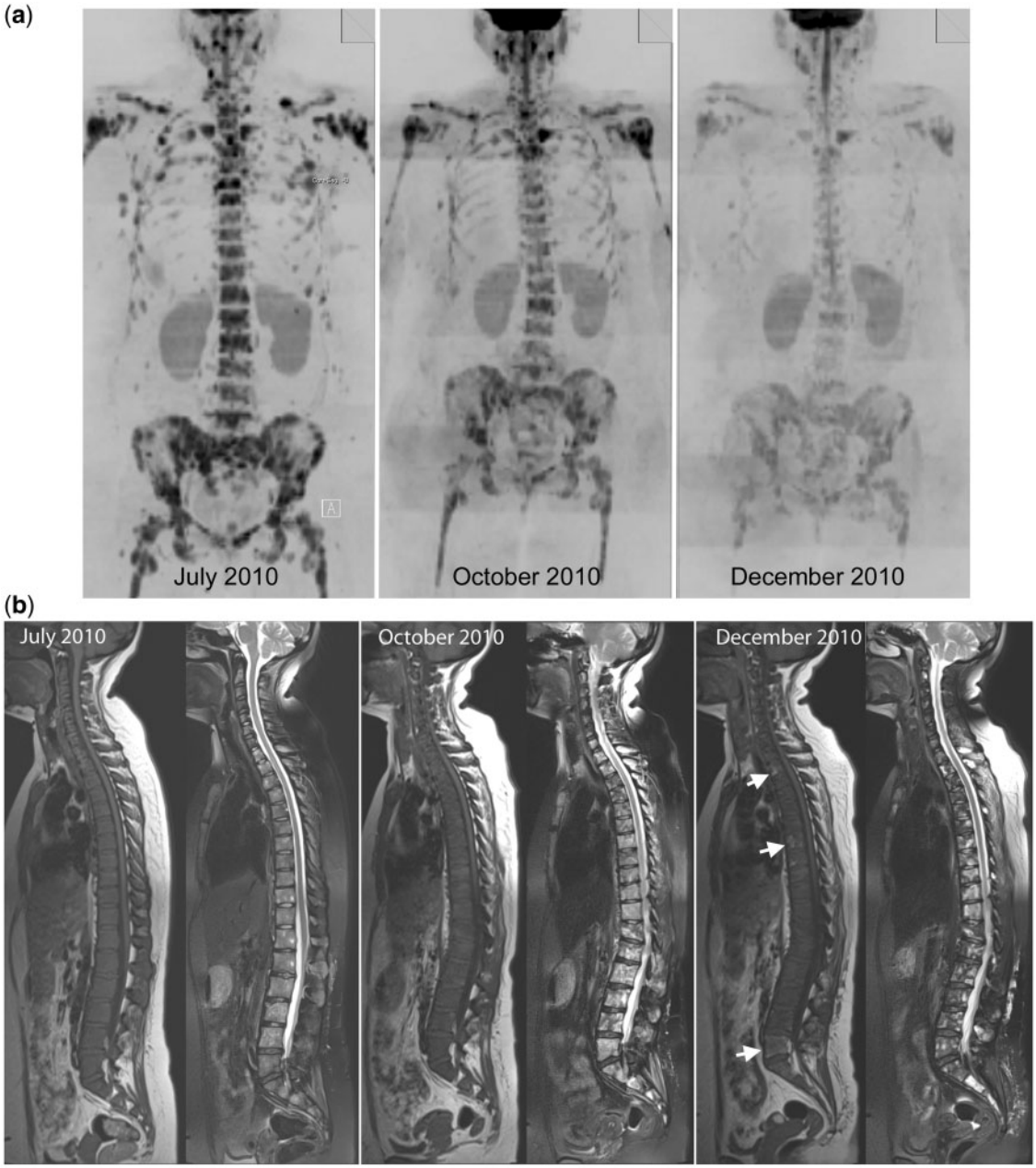

Figure 4 **Disease response in breast cancer. Successful therapy causes decreases in signal intensity on high *b*-value images and increases in ADC values. A 38-year-old woman with triple negative breast cancer treated with gemcitabine and carboplatin chemotherapy and bisphosphonates. (a) Serial b900 3-MIP (inverted scale) images (left panel before therapy, middle panel after 3 months and right panel after 5 months of treatment). There is extensive bony metastatic disease throughout the skeleton at baseline with a diffuse pattern of disease. Serial reductions in the bony marrow signal intensity are observed indicating an overall excellent response to treatment. (b) Serial whole spine sagittal T1W and T2W images. Widespread infiltration of the vertebral bone marrow is evident on T1W images. An increase in signal intensity on T2W images is seen at several levels after 3 months of treatment. It is impossible to tell on T1W imaging whether a response has occurred in the bone marrow. After 5 months of treatment the presence of small amounts of fat within several vertebral bodies (arrows) is observed on T1W images consistent with a healing response. Interval loss of vertebral height at T12 is observed. (c) Axial b900 (left column) and ADC maps (right column) showing marked increases in ADC values of the pelvic bone marrow after treatment. The top panel shows metastatic disease involving the sacrum and iliac bones with a pretherapy mean ADC of 823 $\mu m^2/s$ (SD 162) of the left iliac bone (arrows). The middle panel, 3 months after therapy, shows a mean ADC of 1769 $\mu m^2/s$ (SD 149) at the same level and the lower panel after 5 months shows a mean ADC of 1926 $\mu m^2/s$ (SD 207).**

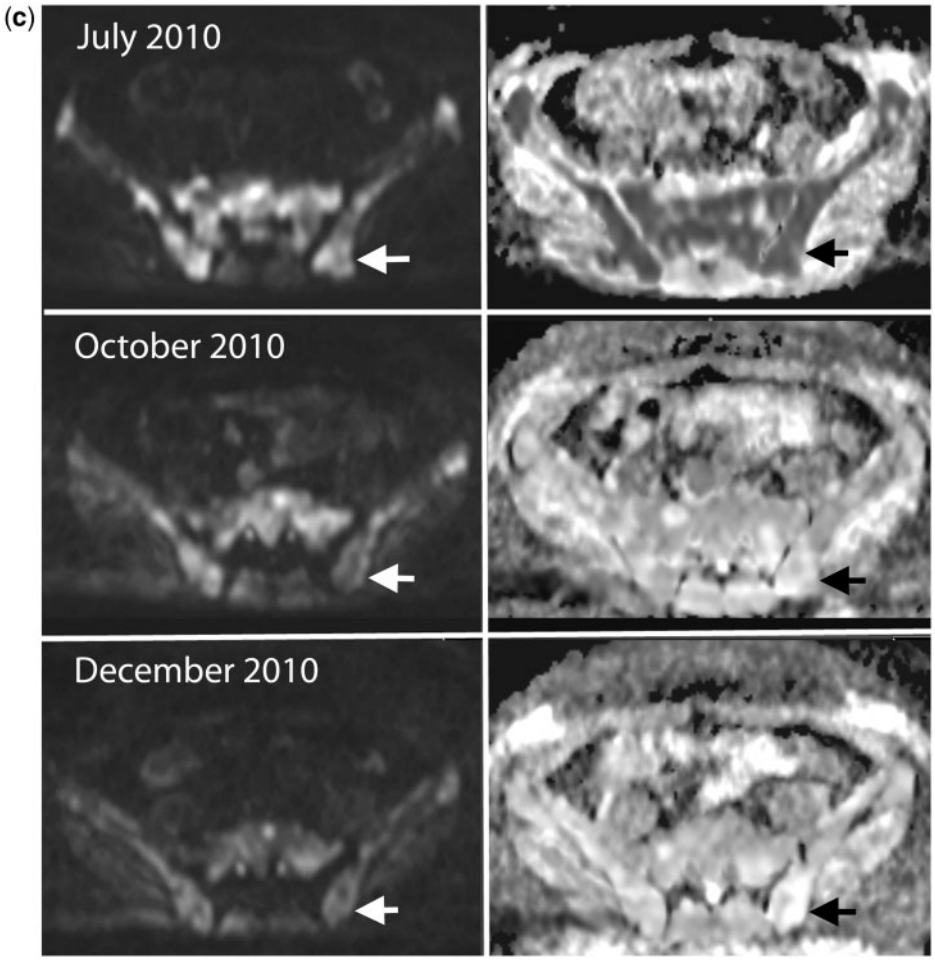

Figure 4 **Continued.**

response. The appearance of bony sclerosis within initially lytic disease in response to therapy can be used to advantage because hyperintense lesions lose signal intensity on WB-DWI. This is because many systemic treatments for osteolytic disease (including denosumab and zoledronic acid) work by inhibiting osteoclastic action, thus converting osteolytic to sclerotic lesions[4,6,8] (and in so doing reduce the frequency of adverse skeletal-related events).

DW-MRI for bone marrow therapy monitoring: mechanisms

Therapy assessments are made by observing changes in the extent, symmetry and intensity of signal on high *b*-value images, corresponding alterations in ADC values, seeking correlations on morphological sequences. When serial studies are being compared across time, then it is important to normalize the signal intensity of the thick maximum intensity projections (MIP) images for effective comparisons to be made. Such normalization may be undertaken by setting the window level to a tissue that is assumed to be unchanging between examinations, then maintaining the window width between examinations. Normalization to the kidney or brain signal is often undertaken for this purpose. Lesion-by-lesion signal intensity and ADC value changes should be interpreted using the guidance given in Table 1. Four general patterns of treatment-induced change can be recognized on WB-DWI.

(1) Disease progression can be determined by observing an increased extent of previously documented disease, as new areas of abnormal signal intensity, or by increases in the intensity of abnormalities on high *b*-value images (Fig. 3). Importantly, bony metastases that progress can have variable changes in ADC values. We have noted slight increases, unchanged or even slight decreases in ADC values compared with pretherapy values[74]. In the setting of disease progression, stability or reductions in ADC values have rational biophysical mechanisms (more tumour of the same type increasing in geographic extent, and increasing tumour cell density (greater number of tumour cells per high power field, limited within a fixed bone marrow space).

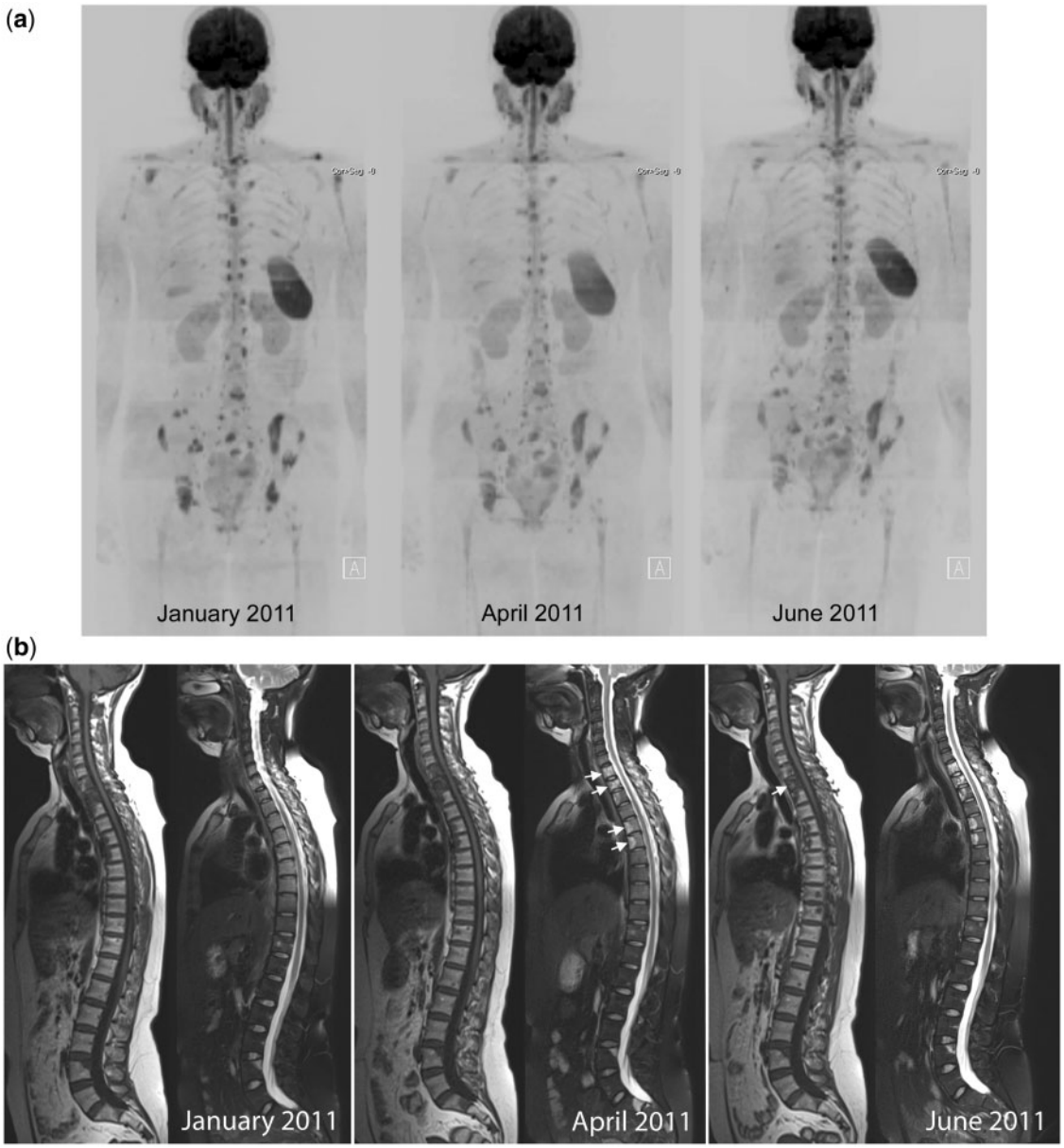

Figure 5 **Disease response in breast cancer. T2-shine through indicating successful response to therapy. A 42-year-old woman with metastatic breast cancer treated with capecitabine and bisphosphonates. (a) Serial b900 3-MIP (inverted scale) images. Left panel before therapy, middle panel after 3 months and right panel after 5 months of treatment. Widespread bony metastatic disease within the vertebral column, ribs, pelvis and proximal femora. No significant alterations in signal intensity of individual lesions are observed post-therapy despite a clinical response to treatment. (b) Serial whole spine sagittal T1W and T2W images. An increase in signal intensity on T2W images within lesions involving the upper dorsal vertebrae at both 3 and 5 months after therapy in keeping with an increase in water content (arrows, middle panel). Lesions appear to have sharper margins on T1W images and have increasing fat content consistent with a healing response (arrow last panel). (c) Axial b900 (left column) and ADC maps (right column) showing marked increases in ADC values of the pelvic bone marrow after treatment. The top panel shows hypercellular metastatic lesions within the sacrum (right-sided arrow) and left iliac bone (left-sided arrow) before therapy shown by increased signal intensity and low ADC values. For example, the mean ADC of the sacral lesion is 882 $\mu m^2/s$ (SD 137) before therapy. The middle and lower panels at 3 and 5 months after treatment demonstrate sustained increases in signal intensity on b900 images but increases in ADC values are seen. The mean ADC within the sacral lesion at 3 months after therapy is 1592 $\mu m^2/s$ (SD 110) and at 5 months is largely unaltered at 1461 $\mu m^2/s$ (SD 209).**

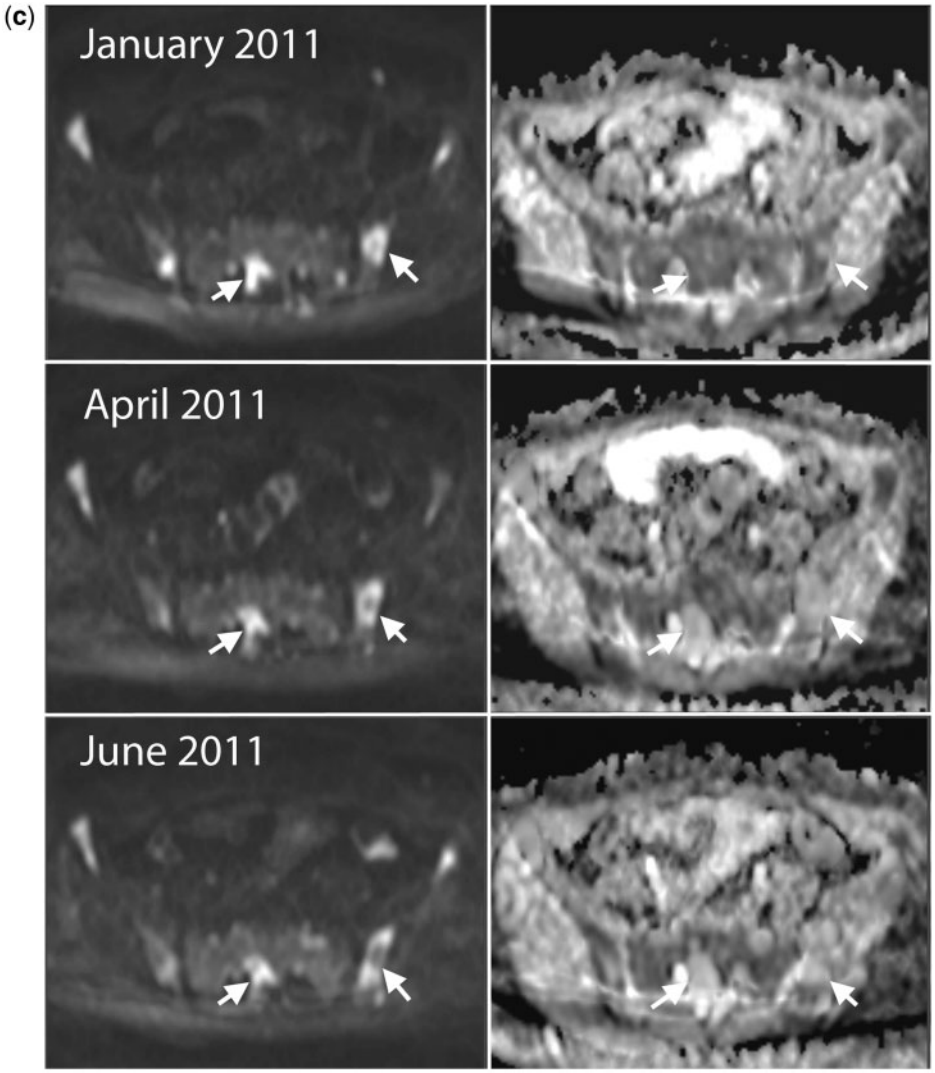

Figure 5 **Continued.**

The causes for slight increases in ADC values have been discussed earlier. In brief, increasing bone marrow tumour infiltration displaces fat cells and increases vascularity, thus returning higher ADC values compared with yellow or mixed bone marrow[52–54,56,57]. The important point to note is that increases in ADC values with progression tend to be of small magnitude provided that the metastatic lesions remain non-necrotic. This is in contrast to bony metastases that respond to treatment, which have much larger increases in ADC values[74]. A practical way of dealing with the variable change in ADC values in order to distinguish response from non-response is to define an upper limit cut-off value of untreated lesions as illustrated in Fig. 1. Readers should note that such cut-off values are likely to be dependent on *b*-value choice and probably on the tumour type.

(2) When bone marrow disease is treated successfully, then tumour cell death results in initial increased water diffusivity manifested as higher ADC values[38,74]. As already mentioned, the magnitude of ADC increases are usually greater than the smaller increases in ADC change seen in disease progression. The extent of ADC increases may be related to the mechanism of tumour cell death induced by the treatment given. It would be expected that ADC increases would be greater for therapies that result in tumour cell kill acting via necrosis mechanisms rather than via apoptosis, although this has not been definitively shown. This is because necrotic cell death is associated with an inflammatory response which is generally not found in tumour cell apoptosis[75]. Regardless of the mechanism of tumour cell death, in the majority of lesions responding to therapy, signal intensity changes on high *b*-value images show decreases (Fig. 4).

(3) Occasionally when there has been a successful response to therapy, marked rise in ADC values are seen but no signal intensity changes are observed. In this situation, bony lesions are of high signal intensity

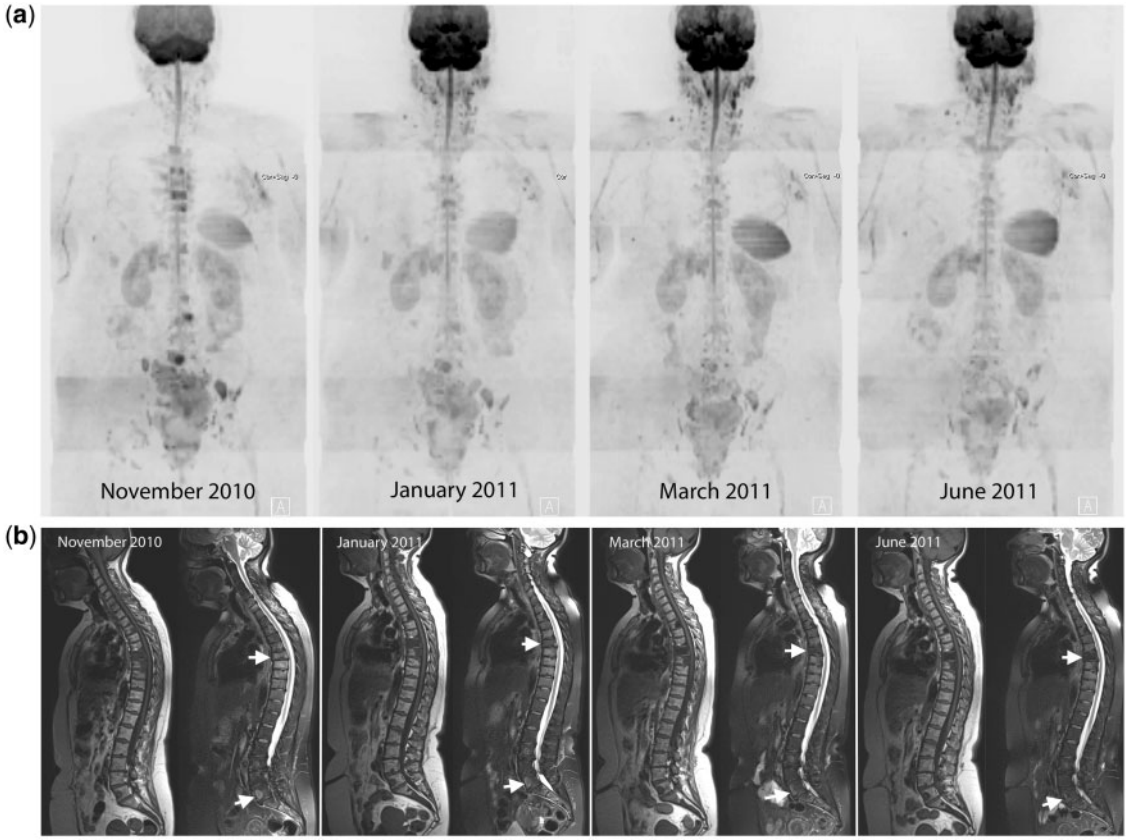

Figure 6 **Clinical response with decreases in signal intensity on high *b*-value images and unchanged ADC values. A 60-year-old woman with metastatic breast cancer treated with capecitabine and bisphosphonates. (a) Serial b900 3-MIP (inverted scale) images. Scans at intervals of approximately 2–3 months after therapy. Reductions in signal intensity in the majority of lesions within the vertebral column and pelvis imply a response to treatment. (b) Serial whole spine sagittal T1W and T2W images. Reduced signal intensity of several vertebral body lesions on T2W imaging on treatment indicates reduced water content and increasing sclerosis of lesions (arrows) consistent with therapy response. (c) Axial b900 (left column) and ADC maps (right column) through the pelvis show reducing signal intensity after therapy of the sacral lesion and of the left iliac lesion (arrows) after therapy. ADC values remain essentially unchanged (left iliac lesion: November 2010, mean 1168 $\mu m^2/s$ (SD 243); March 2011, mean ADC 1164 $\mu m^2/s$ (SD 200); January 2011, mean ADC 1134 $\mu m^2/s$ (SD 137); June 2011, mean ADC 1192 $\mu m^2/s$ (SD 247)).**

and have high ADC values; this is termed T2-shine through. This pattern has been noted particularly in patients with multiple myeloma, lymphoma and occasionally in other solid metastatic neoplasms as illustrated in Fig. 5. The development of T2-shine through in bony lesions should indicate successful therapy response, re-emphasizing the need to always interpret high *b*-values images with corresponding ADC maps, correlating with other imaging findings as necessary. Sometimes, serial follow-up studies are needed to reveal the true nature of response by observing the time course of changes.

(4) The rarest pattern observed is the finding of signal intensity decreases on high *b*-value images with unchanging or slight decreases in ADC values. We have observed this pattern in patients who are clinical responders (Fig. 6) and occasionally in non-responding patients also (Fig. 7). The biophysical mechanisms and therapy implications for these changes early after instituting therapy are unclear with an absence of guidance in the literature. By observing changes in morphological sequences and on CT scans we have noted that increasing calcification of metastases does lead to this appearance (Fig. 7). Since this pattern can be seen in responders and non-responders, these appearances should be considered as indeterminate and currently we resort to morphological and clinical assessments to categorize response.

As already pointed out, the patterns described above are seen soon after instituting therapy. The long-term changes observed on WB-DWI are not well described. At this point it is important to recall that bone marrow disease responding successfully to therapy ultimately results in long-term reductions of signal intensity on high *b*-value images accompanied by reductions in ADC values. This occurs via a number of mechanisms including removal of dead tumour cells, the development

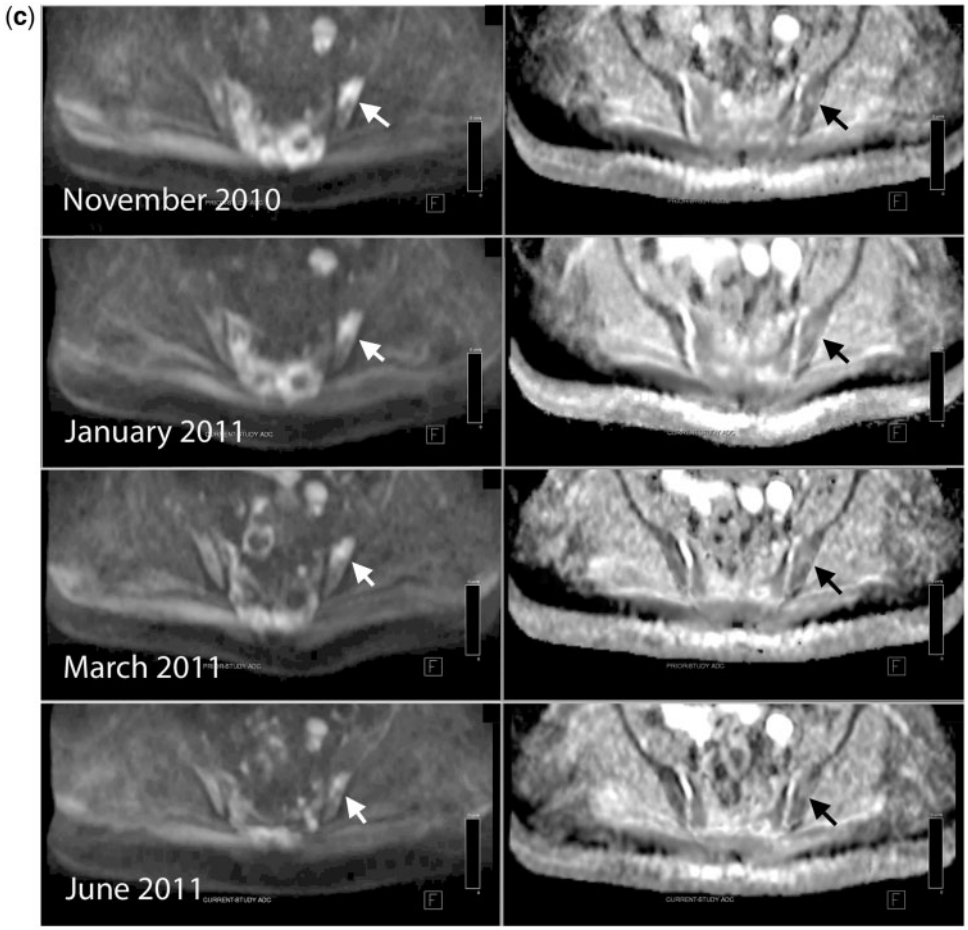

Figure 6 **Continued.**

of bone sclerosis, re-emergence of yellow marrow, loss of tissue water (Fig. 6), secondary myelofibrosis and decreased tissue perfusion[32]. These water diffusivity changes occur slowly, becoming visible many months after starting therapy[76,77], depending on the tumour type and type of therapy administered. Of course, if tumour relapses within the bone marrow then signal intensity on high *b*-value images has corresponding appearances as described above (pattern 1).

DW-MRI for bone marrow therapy assessments: literature review

When bone marrow disease is treated successfully, then tumour cell death results in initial increased water diffusivity manifested as decreases in signal intensity on high *b*-value images and increased ADC values[74,76–80]. DW-MRI of patients with leukaemia have showed marked increase in ADC values and increased diffusivity in areas of necrotic tissue, which suggest successful treatment[79]. A recent study evaluating DW-MRI monitoring of treatment response of vertebral metastatic deposits showed convincing changes from pre-chemotherapy *b*-value hyperintensity to hypointensity following therapy[80]. This study compared DW-MRI with conventional spin echo imaging. The T1W and T2W spin echo follow-up images of spinal metastases revealed no significant interval changes, indicating that they are of limited use in the evaluations of monitoring response to therapy. However, in patients with clinical improvement, the corresponding *b*-values showed demonstrable conversion to hypointensity on subsequent follow-up DW-MRI at the end of therapy. Equally, patients with no clinical improvement demonstrated persistent bone marrow *b*-value hyperintensity suggestive of persistent tumour hypercellularity causing persistent restriction of water diffusion. The clear clinical value of DW-MRI over and above that achieved by conventional T1W and T2W spin echo sequences, perhaps best highlights the advantages of adding DW-MRI sequences to routine protocols.

Conclusions

WB-DWI excels for bone marrow assessments at diagnosis and for therapy evaluations where it can potentially address unmet clinical and pharmaceutical needs for a reliable measure of tumour response. Potentially,

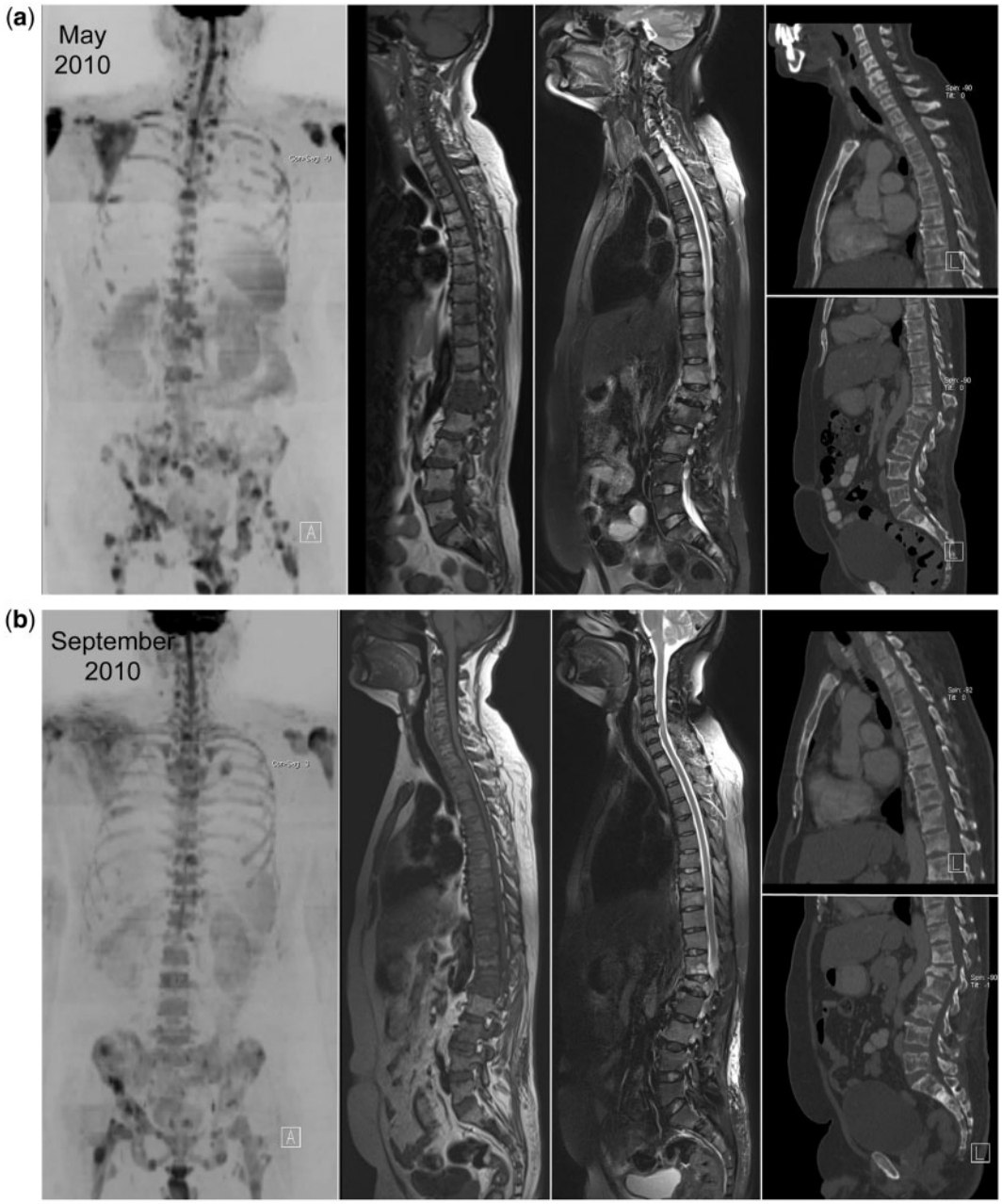

Figure 7 **Disease progression with decreases in signal intensity on high *b*-value images and unchanged ADC values. A 52-year-old man with metastatic prostate cancer treated with docetaxol. (a) b900 3D-MIP (inverted scale), whole spine sagittal T1W and T2W sequences and sagittal reconstructed CT images before therapy. There is widespread lytic and sclerotic bony disease throughout the spine. Metastatic disease involving the pelvis, spine, proximal femora and scapulae are seen. Marked spinal canal narrowing at L1 also. (b) b900 3D-MIP (inverted scale), whole spine sagittal T1W and T2W sequences and sagittal reconstructed CT images 4 months after treatment. Decreases in signal intensity are seen in the majority of lesions on b900 images and increasing bony marrow infiltration on T1W scans. Increasing sclerosis within the vertebral bodies is seen on the CT images. (c) Right scapular images before therapy. Top row: axial STIR, T1W and CT. Bottom row: axial ADC map, b900 and volume-rendered CT image. Metastatic disease involving the right scapula causes bony expansion. The periphery of the lesion is highly cellular (high signal intensity on b900 image and low ADC (mean ADC 1247 $\mu m^2/s$ (SD 263)) with central necrosis. The lesion shows some calcification on the CT images. (d) Right scapular images before therapy 4 months after therapy. Top row: axial STIR, T1W and CT. Bottom row: axial ADC map, b900 and volume-rendered CT image. Reductions in signal intensity on b900 images with unchanging ADC map appearances (mean ADC 1230 $\mu m^2/s$ (SD 403)). The CT study clearly demonstrates increasingly dense calcification of the scapular lesion and bony expansion, indicating sclerotic progression of disease.**

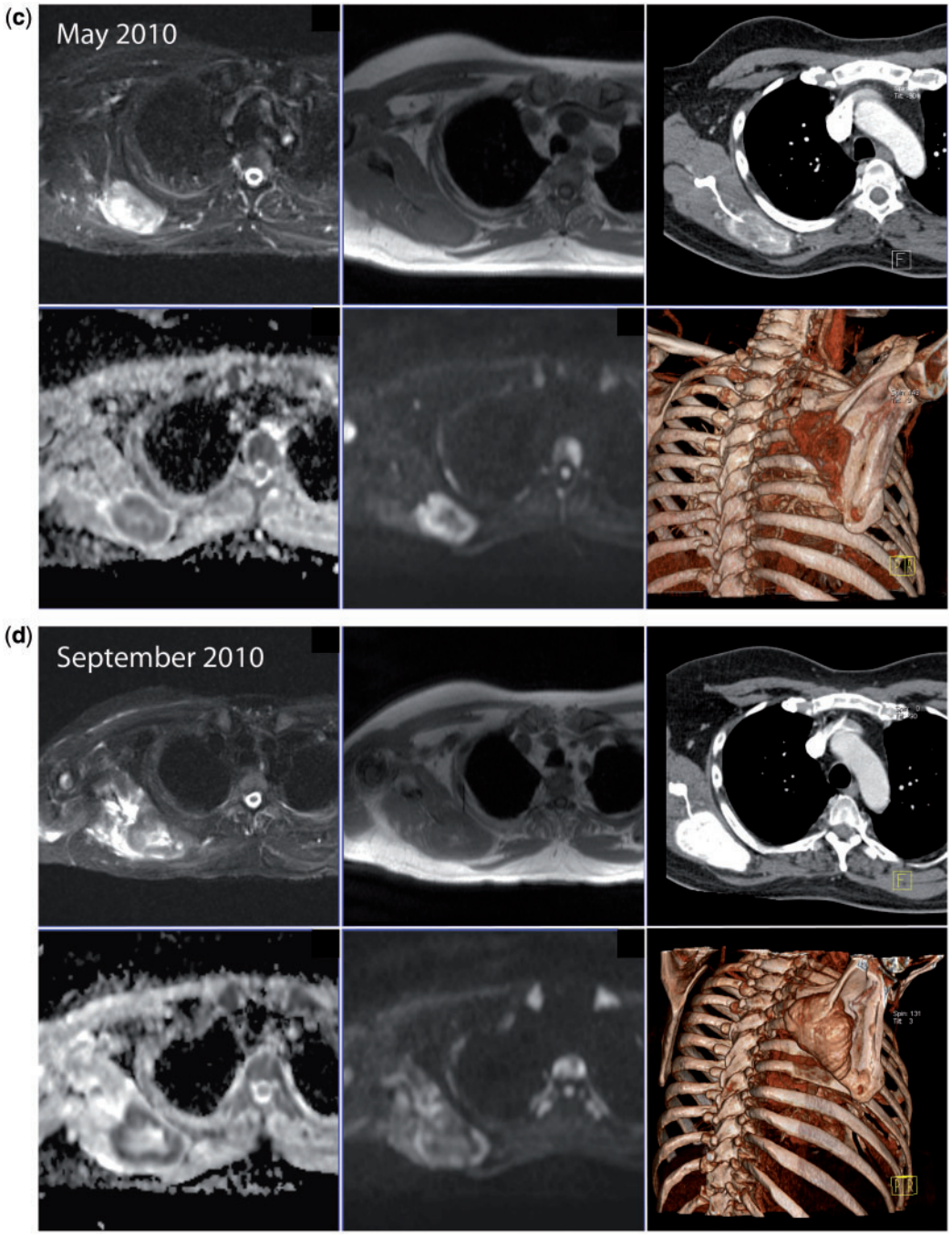

Figure 7 **Continued.**

WB-DWI could make a significant impact in the therapy assessments of patients with metastatic breast and prostate cancer as well as for patients with myeloma. Signal intensity on high *b*-value images and ADC value changes can be related to underlying biophysical properties of skeletal metastases and therapy-induced effects. WB-DWI findings need to be correlated with other complementary anatomic imaging techniques. Therapy response criteria need to be established so that they can be then be tested in prospective clinical studies that incorporate conventional measures of patient benefit. The use of WB-DWI has not yet been proven to impact meaningful health outcomes in patients with skeletal metastases. Thus, although the roles of WB-DWI in patient management are yet to be completely defined, the technology is certainly interesting enough to begin to pursue in the clinic.

References

[1] Abrams HL, Spiro R, Goldstein N. Metastases in carcinoma; analysis of 1000 autopsied cases. Cancer 1950; 3: 74–85.

doi:10.1002/1097-0142(1950)3:1<74::AID-CNCR2820030111>3.0.CO;2-7.

[2] Carlin BI, Andriole GL. The natural history, skeletal complications, and management of bone metastases in patients with prostate carcinoma. Cancer 2000; 88: 2989–94. doi:10.1002/1097-0142(20000615)88:12+<2989::AID-CNCR14>3.0.CO;2-Q.

[3] Coleman RE. Clinical features of metastatic bone disease and risk of skeletal morbidity. Clin Cancer Res 2006; 12: 6243s–9s. doi:10.1158/1078-0432.CCR-06-0931.

[4] Pavlakis N, Schmidt R, Stockler M. Bisphosphonates for breast cancer. Cochrane Database Syst Rev 2005: CD003474.

[5] Body JJ, Bartl R, Burckhardt P, et al. Current use of bisphosphonates in oncology. International Bone and Cancer Study Group. J Clin Oncol 1998; 16: 3890–9.

[6] Lipton A, Small E, Saad F, et al. The new bisphosphonate, Zometa® (zoledronic acid), decreases skeletal complications in both osteolytic and osteoblastic lesions: a comparison to pamidronate. Cancer Invest 2002; 20: 45–54. doi:10.1081/CNV-120014886.

[7] Santini D, Galluzzo S, Zoccoli A, et al. New molecular targets in bone metastases. Cancer Treat Rev 2010; 36(Suppl 3), S6–10. doi:10.1016/S0305-7372(10)70013-X.

[8] Vallet S, Smith MR, Raje N. Novel bone-targeted strategies in oncology. Clin Cancer Res 2010; 16: 4084–93. doi:10.1158/1078-0432.CCR-10-0600.

[9] Clamp A, Danson S, Nguyen H, Cole D, Clemons M. Assessment of therapeutic response in patients with metastatic bone disease. Lancet Oncol 2004; 5: 607–16. doi:10.1016/S1470-2045(04)01596-7.

[10] Scher HI, Halabi S, Tannock I, et al. Design and end points of clinical trials for patients with progressive prostate cancer and castrate levels of testosterone: recommendations of the Prostate Cancer Clinical Trials Working Group. J Clin Oncol 2008; 26: 1148–59. doi:10.1200/JCO.2007.12.4487.

[11] Hamaoka T, Madewell JE, Podoloff DA, Hortobagyi GN, Ueno NT. Bone imaging in metastatic breast cancer. J Clin Oncol 2004; 22: 2942–53. doi:10.1200/JCO.2004.08.181.

[12] Duffy MJ, Evoy D, McDermott EW. CA 15–3: uses and limitation as a biomarker for breast cancer. Clin Chim Acta 2010; 411: 1869–74. doi:10.1016/j.cca.2010.08.039.

[13] Duffy MJ. Serum tumor markers in breast cancer: are they of clinical value? Clin Chem 2006; 52: 345–51. doi:10.1373/clinchem.2005.059832.

[14] Demers LM, Costa L, Lipton A. Biochemical markers and skeletal metastases. Cancer 2000; 88: 2919–26. doi:10.1002/1097-0142(20000615)88:12+<2919::AID-CNCR7>3.0.CO;2-Z.

[15] Dotan E, Cohen SJ, Alpaugh KR, Meropol NJ. Circulating tumor cells: evolving evidence and future challenges. Oncologist 2009; 14: 1070–82. doi:10.1634/theoncologist.2009-0094.

[16] Budd GT, Cristofanilli M, Ellis MJ, et al. Circulating tumor cells versus imaging – predicting overall survival in metastatic breast cancer. Clin Cancer Res 2006; 12: 6403–9. doi:10.1158/1078-0432.CCR-05-1769.

[17] Saad A, Kanate A, Sehbai A, Marano G, Hobbs G, Abraham J. Correlation among [18F]fluorodeoxyglucose positron emission tomography/computed tomography, cancer antigen 27.29, and circulating tumor cell testing in metastatic breast cancer. Clin Breast Cancer 2008; 8: 357–61. doi:10.3816/CBC.2008.n.042.

[18] De Giorgi U, Mego M, Rohren EM, et al. 18F-FDG PET/CT findings and circulating tumor cell counts in the monitoring of systemic therapies for bone metastases from breast cancer. J Nucl Med 2010; 51: 1213–8. doi:10.2967/jnumed.110.076455.

[19] Coleman RE, Mashiter G, Whitaker KB, Moss DW, Rubens RD, Fogelman I. Bone scan flare predicts successful systemic therapy for bone metastases. J Nucl Med 1988; 29: 1354–9.

[20] Ryan CJ, Shah SK, Efstathiou E, et al. Phase II study of abiraterone acetate in chemotherapy-naive metastatic castration-resistant prostate cancer displaying bone flare discordant with serologic response. Clin Cancer Res 2011; 17: 4854–61. doi:10.1158/1078-0432.CCR-11-0815.

[21] Costelloe CM, Chuang HH, Madewell JE, Ueno NT. Cancer response criteria and bone metastases: RECIST 1.1, MDA and PERCIST. J Cancer 2010; 1: 80–92.

[22] Bauerle T, Semmler W. Imaging response to systemic therapy for bone metastases. Eur Radiol 2009; 19: 2495–507. doi:10.1007/s00330-009-1443-1.

[23] Messiou C, Cook G, deSouza NM. Imaging metastatic bone disease from carcinoma of the prostate. Br J Cancer 2009; 101: 1225–32. doi:10.1038/sj.bjc.6605334.

[24] Messiou C, Cook G, Reid AH, et al. The CT flare response of metastatic bone disease in prostate cancer. Acta Radiol 2011; 52: 557–61. doi:10.1258/ar.2011.100342.

[25] Cook GJ. PET and PET/CT imaging of skeletal metastases. Cancer Imaging 2010; 10: 1–8.

[26] Iagaru A, Mittra E, Dick DW, Gambhir SS. Prospective evaluation of (99m)Tc MDP scintigraphy, (18)F NaF PET/CT, and (18)F FDG PET/CT for detection of skeletal metastases. Mol Imaging Biol 2011; doi:10.1007/s11307-011-0486-2.

[27] McCarthy M, Siew T, Campbell A, et al. 18)F-Fluoromethylcholine (FCH) PET imaging in patients with castration-resistant prostate cancer: prospective comparison with standard imaging. Eur J Nucl Med Mol Imaging 2011; 38: 14–22. doi:10.1007/s00259-010-1579-x.

[28] Cook G, Houston S, Rubens R, Maisey M, Fogelman I. Detection of bone metastases in breast cancer by 18FDG PET: differing metabolic activity in osteoblastic and osteolytic lesions. J Clin Oncol 1998; 16: 3375–9.

[29] Fogelman I, Cook G, Israel O, Van der Wall H. Positron emission tomography and bone metastases. Semin Nucl Med 2005; 35: 135–42. doi:10.1053/j.semnuclmed.2004.11.005.

[30] Mortimer JE, Dehdashti F, Siegel BA, Trinkaus K, Katzenellenbogen JA, Welch MJ. Metabolic flare: indicator of hormone responsiveness in advanced breast cancer. J Clin Oncol 2001; 19: 2797–803.

[31] Schmidt GP, Reiser MF, Baur-Melnyk A. Whole-body MRI for the staging and follow-up of patients with metastasis. Eur J Radiol 2009; 70: 393–400. doi:10.1016/j.ejrad.2009.03.045.

[32] Messiou C, deSouza NM. Diffusion weighted magnetic resonance imaging of metastatic bone disease: a biomarker for treatment response monitoring. Cancer Biomark 2010; 6: 21–32.

[33] Vanel D, Casadei R, Alberghini M, Razgallah M, Busacca M, Albisinni U. MR imaging of bone metastases and choice of sequence: spin echo, in-phase gradient echo, diffusion, and contrast medium. Semin Musculoskelet Radiol 2009; 13: 97–103. doi:10.1055/s-0029-1220880.

[34] Messiou C, Collins DJ, Morgan VA, et al. Quantifying sclerotic bone metastases with 2D ultra short TE MRI: a feasibility study. Cancer Biomark 2010; 7: 211–18.

[35] Biffar A, Dietrich O, Sourbron S, Duerr HR, Reiser MF, Baur-Melnyk A. Diffusion and perfusion imaging of bone marrow. Eur J Radiol 2010; 76: 323–8. doi:10.1016/j.ejrad.2010.03.011.

[36] Padhani AR, Koh DM, Collins DJ. Whole body diffusion MR imaging in cancer – current status and research directions. Radiology 2011in press.

[37] Padhani AR, Liu G, Koh DM, et al. Diffusion-weighted magnetic resonance imaging as a cancer biomarker: consensus and recommendations. Neoplasia 2009; 11: 102–25.

[38] Padhani AR, Koh DM. Diffusion MR imaging for monitoring of treatment response. Magn Reson Imaging Clin North Am 2011; 19: 181–209. doi:10.1016/j.mric.2010.10.004.

[39] Manenti G, Di Roma M, Mancino S, et al. Malignant renal neoplasms: correlation between ADC values and cellularity in diffusion weighted magnetic resonance imaging at 3 T. Radiol Med (Torino) 2008; 113: 199–213. doi:10.1007/s11547-008-0246-9.

[40] Hayashida Y, Hirai T, Morishita S, et al. Diffusion-weighted imaging of metastatic brain tumors: comparison with histologic

type and tumor cellularity. AJNR Am J Neuroradiol 2006; 27: 1419–25.
[41] Humphries PD, Sebire NJ, Siegel MJ, Olsen OE. Tumors in pediatric patients at diffusion-weighted MR imaging: apparent diffusion coefficient and tumor cellularity. Radiology 2007; 245: 848–54. doi:10.1148/radiol.2452061535.
[42] Zelhof B, Pickles M, Liney G, et al. Correlation of diffusion-weighted magnetic resonance data with cellularity in prostate cancer. BJU Int 2009; 103: 883–8. doi:10.1111/j.1464-410X.2008.08130.x.
[43] Liu Y, Bai R, Sun H, Liu H, Wang D. Diffusion-weighted magnetic resonance imaging of uterine cervical cancer. J Comput Assist Tomogr 2009; 33: 858–62. doi:10.1097/RCT.0b013e31819e93af.
[44] Sugahara T, Korogi Y, Kochi M, et al. Usefulness of diffusion-weighted MRI with echo-planar technique in the evaluation of cellularity in gliomas. J Magn Reson Imaging 1999; 9: 53–60. doi:10.1002/(SICI)1522-2586(199901)9:1<53::AID-JMRI7>3.0.CO;2-2.
[45] Lyng H, Haraldseth O, Rofstad EK. Measurement of cell density and necrotic fraction in human melanoma xenografts by diffusion weighted magnetic resonance imaging. Magn Reson Med 2000; 43: 828–36. doi:10.1002/1522-2594(200006)43:6<828::AID-MRM8>3.0.CO;2-P.
[46] Ellingson BM, Malkin MG, Rand SD, et al. Validation of functional diffusion maps (fDMs) as a biomarker for human glioma cellularity. J Magn Reson Imaging 2010; 31: 538–48. doi:10.1002/jmri.22068.
[47] Guo AC, Cummings TJ, Dash RC, Provenzale JM. Lymphomas and high-grade astrocytomas: comparison of water diffusibility and histologic characteristics. Radiology 2002; 224: 177–83. doi:10.1148/radiol.2241010637.
[48] Matsubayashi RN, Fujii T, Yasumori K, Muranaka T, Momosaki S. Apparent diffusion coefficient in invasive ductal breast carcinoma: correlation with detailed histologic features and the enhancement ratio on dynamic contrast-enhanced MR images. J Oncol 2010; doi:10.1155/2010/821048.
[49] Wang Y, Chen ZE, Yaghmai V, et al. Diffusion-weighted MR imaging in pancreatic endocrine tumors correlated with histopathologic characteristics. J Magn Reson Imaging 2011; 33: 1071–9. doi:10.1002/jmri.22541.
[50] Nonomura Y, Yasumoto M, Yoshimura R, et al. Relationship between bone marrow cellularity and apparent diffusion coefficient. J Magn Reson Imaging 2001; 13: 757–60. doi:10.1002/jmri.1105.
[51] Tang GY, Lv ZW, Tang RB, et al. Evaluation of MR spectroscopy and diffusion-weighted MRI in detecting bone marrow changes in postmenopausal women with osteoporosis. Clin Radiol 2010; 65: 377–81. doi:10.1016/j.crad.2009.12.011.
[52] Hillengass J, Bauerle T, Bartl R, et al. Diffusion-weighted imaging for non-invasive and quantitative monitoring of bone marrow infiltration in patients with monoclonal plasma cell disease: a comparative study with histology. Br J Haematol 2011; 153: 721–8. doi:10.1111/j.1365-2141.2011.08658.x.
[53] Chan JH, Peh WC, Tsui EY, et al. Acute vertebral body compression fractures: discrimination between benign and malignant causes using apparent diffusion coefficients. Br J Radiol 2002; 75: 207–14.
[54] Messiou C, Collins DJ, Morgan VA, Desouza NM. Optimising diffusion weighted MRI for imaging metastatic and myeloma bone disease and assessing reproducibility. Eur Radiol 2011; 21: 1713–18. doi:10.1007/s00330-011-2116-4.
[55] Chen WT, Shih TT, Chen RC, et al. Vertebral bone marrow perfusion evaluated with dynamic contrast-enhanced MR imaging: significance of aging and sex. Radiology 2001; 220: 213–18.
[56] Chen WT, Shih TT, Chen RC, et al. Blood perfusion of vertebral lesions evaluated with gadolinium-enhanced dynamic MRI: in comparison with compression fracture and metastasis. J Magn Reson Imaging 2002; 15: 308–14. doi:10.1002/jmri.10063.
[57] Pui MH, Mitha A, Rae WI, Corr P. Diffusion-weighted magnetic resonance imaging of spinal infection and malignancy. J Neuroimaging 2005; 15: 164–70. doi:10.1111/j.1552-6569.2005.tb00302.x.
[58] Hwang S, Panicek DM. Magnetic resonance imaging of bone marrow in oncology, Part 1. Skeletal Radiol 2007; 36: 913–20. doi:10.1007/s00256-007-0309-3.
[59] Laor T, Jaramillo D. MR imaging insights into skeletal maturation: what is normal? Radiology 2009; 250: 28–38. doi:10.1148/radiol.2501071322.
[60] Goodsitt MM, Hoover P, Veldee MS, Hsueh SL. The composition of bone marrow for a dual-energy quantitative computed tomography technique. A cadaver and computer simulation study. Invest Radiol 1994; 29: 695–704. doi:10.1097/00004424-199407000-00006.
[61] Vogler JB, , 3rd Murphy WA. Bone marrow imaging. Radiology 1988; 168: 679–93.
[62] Schellinger D, Lin CS, Fertikh D, et al. Normal lumbar vertebrae: anatomic, age, and sex variance in subjects at proton MR spectroscopy: initial experience. Radiology 2000; 215: 910–16.
[63] Syed FA, Oursler MJ, Hefferanm TE, Peterson JM, Riggs BL, Khosla S. Effects of estrogen therapy on bone marrow adipocytes in postmenopausal osteoporotic women. Osteoporos Int 2008; 19: 1323–30. doi:10.1007/s00198-008-0574-6.
[64] Ballon D, Watts R, Dyke JP, et al. Imaging therapeutic response in human bone marrow using rapid whole-body MRI. Magn Reson Med 2004; 52: 1234–8. doi:10.1002/mrm.20291.
[65] Fletcher BD, Wall JE, Hanna SL. Effect of hematopoietic growth factors on MR images of bone marrow in children undergoing chemotherapy. Radiology 1993; 189: 745–51.
[66] Kwee TC, Takahara T, Ochiai R, et al. Whole-body diffusion-weighted magnetic resonance imaging. Eur J Radiol 2009; 70: 409–17. doi:10.1016/j.ejrad.2009.03.054.
[67] Fischer MA, Nanz D, Hany T, et al. Diagnostic accuracy of whole-body MRI/DWI image fusion for detection of malignant tumours: a comparison with PET/CT. Eur Radiol 2011; 21: 246–55. doi:10.1007/s00330-010-1929-x.
[68] Goudarzi B, Kishimoto R, Komatsu S, et al. Detection of bone metastases using diffusion weighted magnetic resonance imaging: comparison with (11)C-methionine PET and bone scintigraphy. Magn Reson Imaging 2010; 28: 372–9. doi:10.1016/j.mri.2009.12.008.
[69] Luboldt W, Kufer R, Blumstein N, et al. Prostate carcinoma: diffusion-weighted imaging as potential alternative to conventional MR and 11C-choline PET/CT for detection of bone metastases. Radiology 2008; 249: 1017–25. doi:10.1148/radiol.2492080038.
[70] Gutzeit A, Doert A, Froehlich JM, et al. Comparison of diffusion-weighted whole body MRI and skeletal scintigraphy for the detection of bone metastases in patients with prostate or breast carcinoma. Skeletal Radiol 2010; 39: 333–43. doi:10.1007/s00256-009-0789-4.
[71] Wu LM, Gu HY, Zheng J, et al. Diagnostic value of whole-body magnetic resonance imaging for bone metastases: a systematic review and meta-analysis. J Magn Reson Imaging 2011; 34: 128–35. doi:10.1002/jmri.22608.
[72] Kwee TC, Takahara T, Niwa T. Diffusion-weighted whole-body imaging with background body signal suppression facilitates detection and evaluation of an anterior rib contusion. Clin Imaging 2010; 34: 298–301. doi:10.1016/j.clinimag.2009.07.006.
[73] Eiber M, Holzapfel K, Ganter C, et al. Whole-body MRI including diffusion-weighted imaging (DWI) for patients with recurring prostate cancer: technical feasibility and assessment of lesion conspicuity in DWI. J Magn Reson Imaging 2011; 33: 1160–70. doi:10.1002/jmri.22542.
[74] Messiou C, Collins DJ, Giles S, et al. Assessing response in bone metastases in prostate cancer with diffusion MRI. International

Society of Magnetic Resonance in Medicine - 19th Annual meeting & Exibition Montreal. 2011; p. 336.

[75] Edinger AL, Thompson CB. Death by design: apoptosis, necrosis and autophagy. Curr Opin Cell Biol 2004; 16: 663–9. doi:10.1016/j.ceb.2004.09.011.

[76] Reischauer C, Froehlich JM, Koh DM, et al. Bone metastases from prostate cancer: assessing treatment response by using diffusion-weighted imaging and functional diffusion maps – initial observations. Radiology 2010; 257: 523–31. doi:10.1148/radiol.10092469.

[77] Messiou C, Collins D, Morgan V, et al. ADC changes with time in focal and diffuse myleoma bone disease as indicators of disease response and progression. Proceedings of the Joint Meeting of International Society of Magnetic Resonance in Medicine and the European Society of Magnetic Resonance in Medicine and Biology. Stockholm, 2010; p. 1716.

[78] Lee KC, Bradley DA, Hussain M, et al. A feasibility study evaluating the functional diffusion map as a predictive imaging biomarker for detection of treatment response in a patient with metastatic prostate cancer to the bone. Neoplasia 2007; 9: 1003–11. doi:10.1593/neo.07954.

[79] Ballon D, Dyke J, Schwartz LH, et al. Bone marrow segmentation in leukemia using diffusion and T(2) weighted echo planar magnetic resonance imaging. NMR Biomed 2000; 13: 321–8. doi:10.1002/1099-1492(200010)13:6<321::AID-NBM651>3.3.CO;2-G.

[80] Byun WM, Shin SO, Chang Y, Lee SJ, Finsterbusch J, Frahm J. Diffusion-weighted MR imaging of metastatic disease of the spine: assessment of response to therapy. AJNR Am J Neuroradiol 2002; 23: 906–12.